A Unified Approach to the Processing of Hyperspectral Images

Bernhard Burgeth[1][0000−0001−6602−6201], Stephan Didas[2][0000−0003−4853−9008], and Andreas Kleefeld[3][0000−0001−8324−821X]

[1] Saarland University, 66123 Saarbrücken, Germany
[2] Trier University of Applied Sciences, Environmental Campus Birkenfeld, 55761 Birkenfeld, Germany
[3] Forschungszentrum Jülich GmbH, Jülich Supercomputing Centre, 52425 Jülich, Germany

Abstract. Since vector fields, such as RGB-color, multispectral or hyperspectral images, possess only limited algebraic and ordering structures they do not lend themselves easily to image processing methods. However, for fields of symmetric matrices a sufficiently elaborate calculus, that includes, for example, suitable notions of multiplication, supremum/infimum and concatenation with real functions, is available. In this article a vector field is coded as a matrix field, which is then processed by means of the matrix valued counterparts of image processing methods. An approximate decoding step transforms a processed matrix field back into a vector field. Here we focus on proposing suitable notions of a pseudo-supremum/infimum of two vectors/colors and a PDE-based dilation/erosion process of color images as a proof-of-concept. In principle there is no restriction on the dimension of the vectors considered. Experiments, mainly on RGB-images for presentation reasons, will reveal the merits and the shortcomings of the proposed methods.

Keywords: multispectral image · hyperspectral image · matrix field · mathematical morphology

1 Introduction

The processing of color images has its intricacies, due to the vectorial nature of the data and the fact that a channel-wise treatment is in general insufficient. This already becomes apparent in the fundamental erosion and dilation processes of mathematical morphology for three-channel images where so-called false-color phenomena occur [21]. Countless attempts have been made to overcome these difficulties with a great variety of methods (see [1, 27] for excellent surveys and [20, 17, 3]), especially for three-channel images, each of it with its own merits and drawbacks. Nevertheless, image processing methods are in great demand for multispectral images or for hyperspectral images. The development of multispectral image processing algorithms is of vital importance in a variety of applications such as in food safety inspections [26], food quality [22, 18, 23],

and in archaelogy [15].
For a typical workflow of the processing of hyperspectral images refer to [16, 28] and the references therein. Often these methods are taylormade for images with a certain fixed number of channels or bands restricting their applicability. The aim of this article is to provide a unified approach to multi-channel images, or vectorial data, for that matter, regardless of their dimension. To this end we assume without loss of generality a multi-channel image as a mapping f of the image domain Ω into the d-dimensional hyper-cube Q^d: $f : \Omega \longmapsto Q^d := [0,1]^d$ with $d \in \mathbb{N}\backslash\{0\}$. Typical examples are gray-value images ($d = 1$) and RGB-color images ($d = 3$). This setting can be achieved if the intensities of each of the d recorded frequencies of the multichannel images are normalized to have values in the interval $[0, 1]$. However, even RGBα-images are considered to belong to this class ($d = 4$), although the meaning of α is not that of a frequency. Nevertheless, in this article we will refer to such a type of image as a (d-dimensional) multi-spectral image, and its values in Q^d often as multi-colors. We will concentrate on providing mathematical concepts applicable to multi-spectral images that allow for the construction of the fundamental building blocks for any numerical image processing algorithm: linear combinations, multiplication, concatenation with functions, and fruitful notions of maximum and minimum. Those key-ingredients are available in the case of so called matrix-fields, where we denote any mapping $F : \Omega \longmapsto \mathrm{SYM}(d)$ from a two- or three-dimensional image domain Ω into the real vector space $\mathrm{SYM}(d)$ of $d \times d$, symmetric matrices as a field of symmetric matrices. For the sake of brevity we will refer to them as $\mathrm{SYM}(d)$-valued images, or even shorter, as $\mathrm{SYM}(d)$-fields. Various methods from scalar image processing have been transferred to the matrix-field setting, resulting in diffusion- or transport-type evolutions of matrix fields, e.g. [7, 11, 12], as well as semi-order-based morphological operations, see [5].
The main idea is to rewrite a multi-spectral image as a $\mathrm{SYM}(d)$-field to take advantage of the image processing concepts available for the later one. Roughly speaking, this "rewriting" of a color vector $c \in Q^d$ amounts to taking its outer or dyadic product with itself $c\,c^\top \in \mathrm{SYM}(d)$. However, one of the challenges will be to reconstruct a multi-spectral image from the processed $\mathrm{SYM}(d)$-field in a reasonable way such that gray-valued mathematical morphology is preserved. The basic structure of the processing strategy is depicted in Fig. 1 in the exemplary case of the pseudo-supremum psup of three-dimensional vectors, resp., their corresponding outer product matrices. Since $\mathrm{SYM}(d)$-fields will play a major role

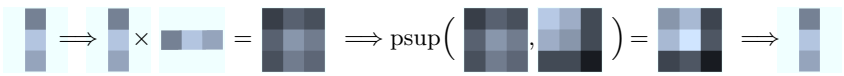

Fig. 1. Proposed processing strategy. Here "⟹" stands for pre- and post-processing.

in the sequel, the necessary rudiments of matrix fields and their calculus will be presented in the subsequent section. For further details the reader is referred

to [11, 12]. We will describe the coding of a multi-spectral image and the corresponding decoding of the matrix field in section 3. Based on [11] we provide in section 4 a short introduction to matrix-valued counterparts of the morphological PDEs of dilation and erosion and their numerical solution schemes. In section 5 we report on experiments performed mainly on three-channel images and on higher dimensional multi-spectral signals as a proof-of-concept, while the last section 6 is devoted to concluding remarks and an outlook.

2 Rudiments of a Calculus for Symmetric Matrices

For the sake of brevity, we present here only the very basic notions from calculus of symmetric matrices: For details see [5] and [7]. Any matrix $S \in \text{SYM}(d)$ can be diagonalized by means of a suitable orthogonal matrix and, furthermore, all the eigenvalues are real: $S = QDQ^\top$. Here, Q is orthogonal, that is, $Q^\top Q = QQ^\top = I$ and $D = \text{diag}(\lambda_1, \ldots, \lambda_n)$ is a diagonal matrix with real entries in decreasing order, $\lambda_1 \geq \ldots \geq \lambda_d$. The matrix S is called positive semidefinite if $\lambda_1 \geq \ldots \geq \lambda_d \geq 0$. We will call a matrix with this property a spd-matrix. If the eigenvalues are strictly positive, the matrix is called positive definite. A matrix S is negative (semi-)definite if $-S$ is positive (semi-)definite. If the matrix S is none of the above, then the symmetric matrix is called indefinite. This gives rise to a partial order "$\geq$" on $\text{SYM}(d)$, often referred to as Loewner order (refer to [2]):

$$A \geq B \text{ if and only if } A - B \text{ is positive semidefinite.}$$

Note that $\text{SYM}(d)$ with this order is not a lattice. Nevertheless, as it is pointed out in [6], and in more detail in [5, 8], a rich functional algebraic calculus can be set up for symmetric matrices. This allows to establish numerous filtering and analysis methods for such fields in a rather straight forward manner from their scalar counterparts [11]. We call the matrices $\text{psup}(A, B)$ and $\text{pinf}(A, B)$ as defined in Table 1 for $A, B \in \text{SYM}(d)$ pseudo-supremum resp., pseudo-infimum. They are the upper, resp., lower matrix valued bounds of smallest, resp., largest trace, and as such, acceptable replacements for supremum/infimum in this non-lattice setting, see [10].

3 From Hyperspectral Image to Matrix Field and Back

In this section, we will elaborate on embedding vectorial data of a hyperspectral image into a field of symmetric matrices, and on the restoration of a hyperspectral image from a (processed) field of positive, symmetric matrices. The key is the following simple observation:
Suppose the column vector $0 \neq c = (c_1, \ldots, c_d) \in Q^d$ codes a multi-color, then the outer or dyadic product $cc^\top$ is a matrix which is non-negative, symmetric, and has rank one. It can be seen as a very special autocorrelation matrix of the vector c. The only non-zero eigenvalue r satisfies $r = \|c\|_2^2 = \text{trace}(cc^\top)$. Keeping in mind that $\|c\|_\infty \leq 1 \longleftrightarrow c \in Q^d$, it is not difficult to reconstruct

Table 1. Transferring elements of scalar valued calculus (middle) to the symmetric matrix setting (right).

setting	scalar valued	matrix-valued
function	$f : \begin{cases} \mathbb{R} \longrightarrow \mathbb{R} \\ x \mapsto f(x) \end{cases}$	$F : \begin{cases} \mathrm{SYM}(d) \longrightarrow \mathrm{SYM}(d) \\ S \mapsto Q\mathrm{diag}(f(\lambda_1), \ldots, f(\lambda_d))\, Q^\top \end{cases}$
partial derivatives	$\partial_\omega g,$ $\omega \in \{t, x_1, \ldots, x_d\}$	$\overline{\partial}_\omega S := (\partial_\omega s_{ij})_{ij},$ $\omega \in \{t, x_1, \ldots, x_d\}$
gradient	$\nabla g(x) := (\partial_{x_1}\ g(x), \ldots, \partial_{x_d}\ g(x))^\top,$ $\nabla h(x) \in \mathbb{R}^d$	$\overline{\nabla} G(x) := (\overline{\partial}_{x_1}\ G(x), \ldots, \overline{\partial}_{x_d}\ G(x))^\top,$ $\overline{\nabla} H(x) \in (\mathrm{SYM}(d))^d$
length	$\lvert h\rvert_p := \sqrt[p]{\lvert h_1\rvert^p + \cdots + \lvert h_d\rvert^p},$ $\lvert h\rvert_p \in [0, +\infty[$	$\lvert H\rvert_p := \sqrt[p]{\lvert H_1\rvert^p + \cdots + \lvert H_d\rvert^p},$ $\lvert H\rvert_p \in \{M \in \mathrm{SYM}(d) \mid M \geq 0\}$
product	$a \cdot b$	$A \bullet B = \frac{1}{2}(AB + BA)$
supremum	$\sup(a, b)$	$\mathrm{psup}(A, B) = \frac{1}{2}(A + B + \lvert A - B\rvert)$
infimum	$\inf(a, b)$	$\mathrm{pinf}(A, B) = \frac{1}{2}(A + B - \lvert A - B\rvert)$

the original color vector by performing (theoretically) a spectral decomposition on $cc^\top$, providing us with a unique eigenvector v, which belongs to the largest eigenvalue r, has non-negative entries and euclidean length $\|v\|_2 = \sqrt{r}$. Then $v = c$ holds. However, between coding and decoding the actual processing happens, confronting us with matrices of higher than rank one. Although this effect cannot be avoided completely, some pre- and post-processing steps are in order.

3.1 Vector Data to Matrix Field

The pre-, resp., post-processing of a (multi-)color vector c requires several, notably reversible steps.

1. Renormalization of the color vector c. Let $B_p = \{v \in \mathbb{R}^d \,|\, \|v\|_p \leq 1\}$ denote the unit ball in $\mathbb{R}^d$ with respect to the p-norm, $p \in [1, \infty]$. Then $Q^d = B_\infty \cap \{v \in \mathbb{R}^d \,|, v_1, \ldots, v_d \geq 0\}$. The function
$$\psi \,:\, v \longmapsto \frac{\|v\|_\infty}{\|v\|_2} \cdot v$$
maps Q^d to $B_2 \cap \{v \in \mathbb{R}^d \,|, v_1, \ldots, v_d \geq 0\}$.
2. This transform is invertible, with
$$\psi^{-1} \,:\, v \longmapsto \frac{\|v\|_2}{\|v\|_\infty} \cdot v\,.$$

The coding of a multispectral image as a matrix field is done by a mapping Φ defined as follows.

Definition 1. *Let $f : \Omega \longmapsto Q^d$ be a d-dimensional multispectral image. Then define a mapping Φ by*

$$\Phi : \begin{cases} Q^d \longrightarrow \mathrm{SYM}(d) \\ c \quad \longmapsto \psi(c) \cdot \psi(c)^\top \end{cases}$$

To each multispectral image f one associates a matrix field $F : \Omega \longrightarrow \mathrm{SYM}(d)$ simply by concatenating Φ and f: $F := \Phi \circ f$.

Writing in short $\psi = \psi(f(x))$ the matrix $F(x) = \Phi(f(x))$ of the color $c = f(x)$ at pixel x has the form

$$F(x) = \Phi(c) = \begin{pmatrix} \psi_1^2 & \cdots & \psi_1\psi_d \\ \vdots & \ddots & \vdots \\ \psi_1\psi_d & \cdots & \psi_d^2 \end{pmatrix} .$$

Note that the normalisation step pays tribute to the fact that the approach relying on the scalar and outer product is closly related to the Euclidean norm rather than the infinity norm the cube Q^d alludes to. Next, we list a few properties of the matrix $\Phi(c)$.

1. The matrix $\Phi(c)$ has rank 1, and is a positive semidefinite matrix.
2. Due to the renormalization of c via ψ, the matrix $\Phi(c) = \psi(c)\cdot\psi(c)^\top$ satisfies $\mathrm{trace}(\Phi(c)) \leq 1$ for any color $c \in Q^d$.
3. If $\|c\|_\infty = 1$, then $\mathrm{trace}(\Phi(c)) = 1$.
4. A closer look at the construction of ψ and Φ reveals that ψ and Φ are positive-homogeneous of degree 1 and 2, respectively:
   $\psi(t \cdot c) = |t|\psi(c)$ and $\Phi(t \cdot c) = |t|^2\Phi(c)$ for $t \in \mathbb{R}$.
5. The function ψ^{-1} is positive-homogeneous as well.
6. v is a (right-)eigenvector of $\Phi(v)$ with the only non-zero eigenvalue $\|v\|^2$.
7. It is important to note that any positive semidefinite rank-1-matrix can be written as an outer product of a vector v or $-v$ with itself. Hence, we can recover the generating vector uniquely from a positive semidefinite rank-1-matrix via spectral decomposition and requiring that e.g. the last component $v_d \geq 0$. In other words, Φ can be assumed invertible on its range $\Phi(Q^d)$.

Gray-scale images are captured in the multispectral setting by the specification $t \cdot (1, \ldots, 1)$ with $t \in [0, 1]$. Therefore, it is this homogeneity that will ensure the preservation of basic gray-value morphology by the proposed approach. In the next section, we address the decoding, that is, transforming a spd-matrix field back into a proper hyperspectral image.

3.2 Matrix Field to Vector Data: Approximate Inverse of σ

For the decoding of a spd-matrix consisting of rank-1-matrices we simply may use the inverse Φ^{-1} available for rank-1-matrices (only). However, in general, the processing of matrix-fields does not preserve neither the rank-1- nor the spd-property of its matrices. Precisely, it can happen that the pseudo-supremum and pseudo-infimum of two rank-1 matrices is not rank-1. Hence, we have to make do with an approximate inverse mapping $\Phi^{\leftarrow}$. The construction of $\Phi^{\leftarrow}$ boils down to extracting from a general $\mathrm{SYM}(d)$-field a field with symmetric rank-1-matrices. To this end suppose that $F(x)$ is a symmetric matrix at location x. The Eckart-Young-Mirsky theorem (see [13, 14]) provides us with the best rank-1 approximation of $F(x)$ with respect to the Frobenius-Norm for matrices: if $\lambda_{\max}(x)$ is the largest eigenvalue (by absolute value) in the spectrum of $F(x)$ and $v(x)$ is a corresponding eigenvector with $\|v(x)\|_2 = 1$ then

$$F^*(x) := \lambda_{\max}(x)\, v(x)v^\top(x)\,.$$

The transition $F(x)$ to $F^*(x)$ is achieved by terminating the spectral decomposition of $F(x)$ with the first summand:

$$F(x) = \sum_{i=1}^{d} \lambda_i\, v_i(x)v_i(x)^\top \approx \lambda_{\max}(x)\, v(x)v(x)^\top = F^*(x)\,,$$

where $(\lambda_i)_{i=1,\dots,d}$ is arranged in decreasing order. This is a linear projection, hence, positive homogeneous.
From this field F^* we may extract a vector $\Phi^{\leftarrow}(F^*(x)) = \sqrt{\lambda_{\max}(x)}\, v(x)$ (according to property 6). Finally, we may apply the positively homogeneous ψ^{-1} to such a vector hence obtaining a new vector

$$\begin{aligned}\psi^{-1}\Big(\Phi^{\leftarrow}(F^*(x))\Big) &= \psi^{-1}(\sqrt{\lambda_{\max}(x)}\, v(x)) = \sqrt{\lambda_{\max}(x)}\cdot\psi^{-1}(v(x)) \\ &= \sqrt{\lambda_{\max}(x)}\, w(x)\end{aligned}$$

as a candidate for the processed color vector at x.

Remark 1. Due to the "geometry" of pseudo-supremum/infimum as a mapping on symmetric matrices, see [9], numerical experiments revealed that

$$1 < \mathrm{trace}(F^*(x)) = \lambda_{\max}(x) \leq 1.05, \quad \text{for } d = 3$$

entailing $\sqrt{\lambda_{\max}(x)}w(x) \notin Q^d$ does not represent a color by a small margin. A fast and "homogeneous" remedy is a rescaling of the rank-1-matrix $F^*(x)$ with a factor $\Big(\max(1, \sqrt{\lambda_{\max}(x)})\Big)^{-1}$. Since this happens only for nearly "antagonistic" colors $c_1, c_2 \in Q^d$ with $c_1 + c_2 = (1, \dots, 1)$ a simple cut-off is a possibly more convenient choice.

4 Basic PDE-Driven Morphology

The correspondence between real and matrix calculus allows to formulate matrix valued partial differential equations (PDEs), and even matrix valued solution schemes may be gleaned from the real-valued counterparts [5], [11].

4.1 Continuous Morphology: Matrix-Valued PDEs

The matrix valued equivalent of the morphological PDEs ([4, 24]) for dilation (+) and erosion (−) proposed for symmetric matrices U in [5] reads for $U(x,t) \in \mathrm{SYM}(d)$:

$$\overline{\partial}_t U = \pm |\overline{\nabla} U|_2 \tag{1}$$

with $U(x,t) \in \Omega \times [0,\infty)$. We refer to Table 1 for the bar and norm notation.

4.2 Continuous Morphology: Matrix-Valued Solution Scheme

Due to its simplicity we extend the first-order upwind scheme of Rouy and Tourin [19, 25] (RT-scheme) from gray-scale images to the matrix setting to solve (1). We denote by u_{ij}^n the gray value of the image u at the pixel centered at $(ih_x, jh_y) \in \Omega \subset \mathbb{R}^2$ at the time-level $n\tau$ of the evolution with time-step $\tau > 0$. The RT-scheme is expressed in a form that allows directly to extend the coding procedure to the 3D matrix valued setting of $\mathrm{SYM}(d)$:

- Instead of gray values u_{ij}^n we employ symmetric matrices $U^n(ih_x, jh_y)$.
- The max-function used below in a scalar-valued setting, is replaced by its matrix-valued generalization psup as given in Table 1, and we proceed likewise with the min-function and pinf.
- The equation can be extended without major difficulties to 3D matrix fields $U^n(ih_x, jh_y, kh_z)$.

For the sake of brevity we restrict ourselves to morphological dilation, the scheme for erosion involves only a simple switch of sign, see (1). The abbreviations we use for forward and backward difference operators are standard, i.e.,

$$D_+^x u_{i,j}^n := u_{i+1,j}^n - u_{i,j}^n \quad \text{and} \quad D_-^x u_{i,j}^n := u_{i,j}^n - u_{i-1,j}^n \,. \tag{2}$$

These operators can be defined analogously with respect to the y-direction. The Rouy-Tourin scheme we exploit here reads

$$u_{i,j}^{n+1} = u_{i,j}^n + \tau \left(\max\left(\frac{1}{h_x} \max\left(-D_-^x u_{i,j}^n, 0\right) \,,\, \frac{1}{h_x} \max\left(D_+^x u_{i,j}^n, 0\right) \right)^2 \right.$$
$$\left. + \quad \max\left(\frac{1}{h_y} \max\left(-D_-^y u_{i,j}^n, 0\right) \,,\, \frac{1}{h_y} \max\left(D_+^y u_{i,j}^n, 0\right) \right)^2 \right)^{1/2} \tag{3}$$

Its performance is very similar to that of the first-order version of a scheme of Osher and Sethian. With this machinery at our disposal we will not process fields of symmetric matrices for their own sake, however. Instead, a color image is coded as a $\mathrm{SYM}(d)$-field with suitable $d = 2, 3, \ldots$ and processed in this "detour space" before being transformed back.

5 Numerical Issues and Experiments

A convenient way to calculate the dominating eigenpair (eigenvalue end eigenvector) is the robust power method. This method is suited to our setting as we may expect a small ratio of second largest to largest eigenvalue for the matrices encountered here. The use of a complete spectral decomposition algorithm is to costly while unnecessary especially with large matrices resulting from high-dimensional multi-spectral images. In a first set of experiments we calculate the $\mathrm{psup}(c_1, c_2)$, resp. $\mathrm{pinf}(c_1, c_2)$ of a pair of colors c_1, c_2. The first experiments are concerned with gray-scales, the results confirm that the proposed approach indeed preserves gray-value morphology. This property is a direct consequence

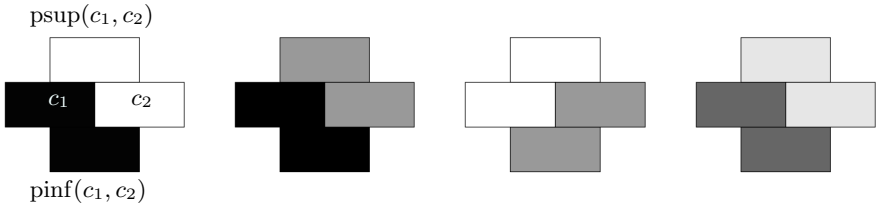

Fig. 2. The p-supremum of two gray values coincides with the maximum of the two. The same holds true for their p-infimum resp. minimum.

of the homogeneity of both the transformation of a color vector into a matrix and the pre- resp. post-processing. Black and white are the extreme gray-values, as expected. This remains true when a color, for example blue, is involved, as can be seen in Fig. 3. However, some results for pairs of colors spaced further

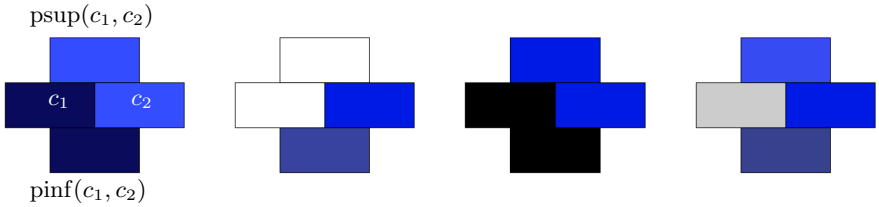

Fig. 3. The p-supremum/infimum involving the color blue. The p-supremum of the two shades of blue coincides with their maximum. The same holds true for their p-infimum resp. minimum.

apart in the RGB-cube are less intuitive, as Fig. 4 reveals. Still, the role of black and white as extreme colors is supported. The outer product of two vectors is a non-linear mapping, hence, it might be instructive to compare the linear combination of two colors (as vectors) with the pseudo-combination of colors via the matrix-valued setting. Some results are depicted in Fig. 5. In Fig. 6 processing of a real-world RGB image with our method is displayed. It is clearly visible

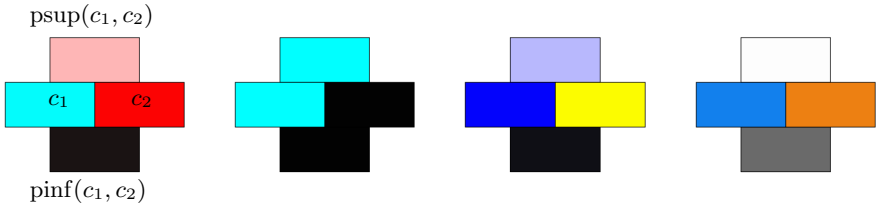

Fig. 4. P-supremum, p-infimum of colors differing significantly in the RGB-cube.

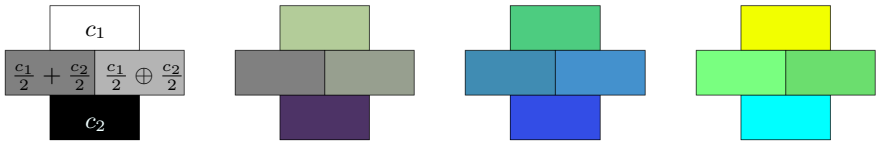

Fig. 5. Averages of pairs of colors c_1, c_2: standard average $\frac{c_1}{2} + \frac{c_2}{2}$ vs. average of the corresponding matrices, indicated by $\frac{c_1}{2} \oplus \frac{c_2}{2}$.

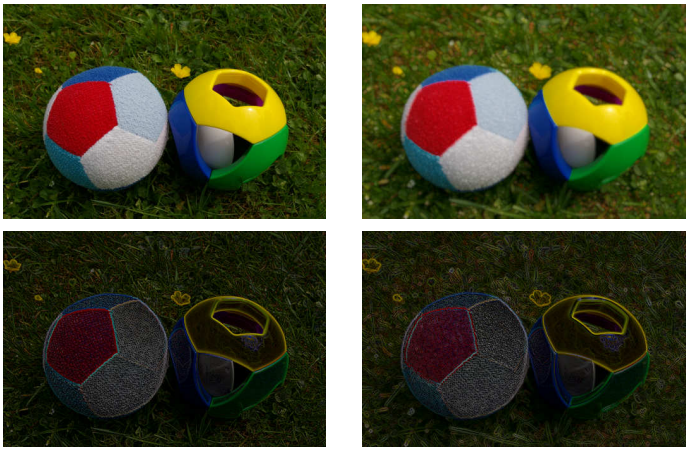

Fig. 6. Morphology on real-world color images. *Top left:* Original image, 512 × 340 pixels, RGB. *Top right:* Dilation with stopping time $t = 2$. *Bottom left:* Internal gradient with stopping time $t = 1$. *Bottom right:* External gradient with stopping time $t = 1$.

that the dilation, internal gradient and external gradient behave as expected for color images. Our second experiment with real-world data displays a section of a printed circuit board with electronic components and labels (cf. Fig. 7). With a white top hat, small bright structures in different colors on darker background, like the conductor paths or the component labelling, are extracted. A morphological shock filter locally choses an dilation or erosion, depending on the sign of the dominant eigenvalue of the morphological Laplacian and clearly sharpens the edges of the image. Of course, the question remains whether the new colors make sense from the perceptional point of view. Proceeding to the multi-

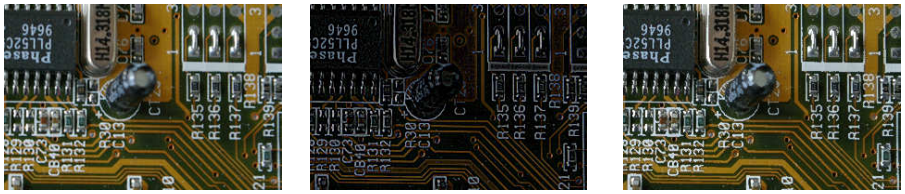

Fig. 7. Morphology on real-world color images. *Left:* Original image, 300×200 pixels, RGB. *Middle:* White top hat with stopping time $t = 1$. *Right:* Morphological shock filter with stopping time $t = 1$.

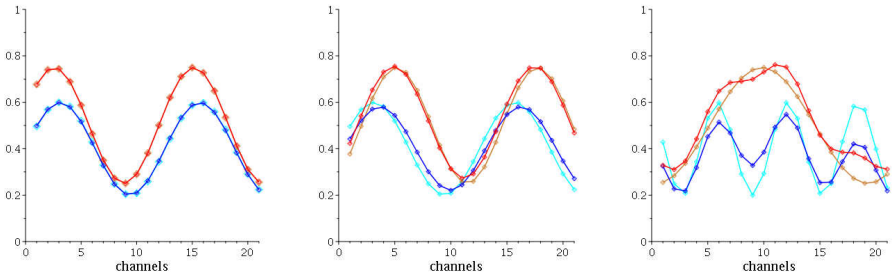

Fig. 8. Images show the performance of the proposed method for some pairs of multicolors, starting from "separated" colors (left) reaching over "weakly separated" (middle) to "interlaced" colors (right). Cyan and gold color indicate the original multicolor, while red and blue represent their pseudo-supremum, resp., pseudo-infimum. In the "separated" case left, p-supremum and p-infimum cover the original multi-colors.

channel case, we represent multi-colors as points in a $x - y-$coordinate system, each point representing a channel. The first experiment in Fig. 8 (left) justifies that the pseudo-supreum/pseudo-infimum of two multi-colors deserve their name: if one vector dominates the other componentwise, their pseudo-supremum coincides with the dominating one, while the pseudo-infimum is equal to the dominated vector. However, the proposed method does not act componentwise, hence, some counter-intuitive results might occur, as further experiments reveal, see Fig. 8. We will use the matrix valued version of the Rouy-Tourin-scheme, m-RT-scheme for short, to perform PDE-driven dilation processes in the "detour"-space $\mathrm{Sym}(d)$. A further investigation how the method scales complexity-wise when the number of channels increases to hundreds has to be investigated in the future.

6 Summary

The proposed unifying approach to the processing of vector valued data, such as color- and multi-spectral images, takes advantage of the methods already available for fields of symmetric matrices. A vector field is coded as a matrix

field which is then processed and finally transformed back into a vector field. However, the embedding of a vector field into a matrix field via the outer product of vectors requires pre- and post-processing of the results to allow for a consistent reconstruction of the vectors from the matrices in such a way that gray scale images (as special color-images) are processed according to standard gray-value morphology. Indeed, the methods presented boil down to gray value morphology when applied to gray-scale images. The experiments confirm the applicability of the methods to RGB-images and indicate their conceptual usefulness in the case of multispectral data. Future research will deal with challenging applications to real hyperspectral images, the intricacies of the pre- and post-processing, and, most importantly, the modeling of inter-channel correlations.

References

1. Aptoula, E., Lefèvre, S.: A comparative study on multivariate mathematical morphology. Pattern Recognition **40**(11), 2914–2929 (2007)
2. Bhatia, R.: Matrix Analysis. Graduate Texts in Mathematics, Springer, New York (1996)
3. Braun, K.M., Balasubramanian, R., Eschbach, R.: Development and evaluation of six gamut-mapping algorithms for pictorial images. In: Color Imaging Conference. pp. 144–148. IS&T - The Society for Imaging Science and Technology (1999)
4. Brockett, R.W., Maragos, P.: Evolution equations for continuous-scale morphology. In: Proc. IEEE International Conference on Acoustics, Speech and Signal Processing. vol. 3, pp. 125–128. San Francisco, CA (Mar 1992)
5. Burgeth, B., Bruhn, A., Didas, S., Weickert, J., Welk, M.: Morphology for tensor data: Ordering versus PDE-based approach. Image and Vision Computing **25**(4), 496–511 (2007)
6. Burgeth, B., Bruhn, A., Papenberg, N., Welk, M., Weickert, J.: Mathematical morphology for tensor data induced by the Loewner ordering in higher dimensions. Signal Processing **87**(2), 277–290 (Feb 2007)
7. Burgeth, B., Didas, S., Florack, L., Weickert, J.: A generic approach to diffusion filtering of matrix-fields. Computing **81**, 179–197 (2007)
8. Burgeth, B., Didas, S., Florack, L., Weickert, J.: A generic approach to the filtering of matrix fields with singular PDEs. In: Sgallari, F., Murli, F., Paragios, N. (eds.) Scale Space and Variational Methods in Computer Vision, Lecture Notes in Computer Science, vol. 4485, pp. 556–567. Springer, Berlin (2007)
9. Burgeth, B., Kleefeld, A.: An approach to color-morphology based on einstein addition and loewner order. Pattern Recognition Letters **47**, 29–39 (2014)
10. Burgeth, B., Kleefeld, A.: Towards processing fields of general real-valued square matrices. In: Hotz, I., Özarslan, E., Schultz, T. (eds.) Modeling, Analysis, and Visualization of Anisotropy. Springer, Heidelberg (2017)
11. Burgeth, B., Pizarro, L., Breuß, M., Weickert, J.: Adaptive continuous-scale morphology for matrix fields. International Journal of Computer Vision **92**(2), 146–161 (2011)
12. Burgeth, B., Pizarro, L., Didas, S., Weickert, J.: 3d-coherence-enhancing diffusion filtering for matrix fields. In: Florack, L., Duits, R., Jongbloed, G., van Lieshout, M.C., Davies, L. (eds.) Mathematical Methods for Signal and Image Analysis and Representation, pp. 49–63. Springer, London (2012)

13. Eckart, C., Young, G.: The approximation of one matrix by another of lower rank. Psychometrika **1**(1), 211–218 (1936)
14. Golub, G.H., Hoffman, A., Stewart, G.W.: A generalization of the eckart-young-mirsky matrix approximation theorem. Linear Algebra and its Applications **88–89**, 317–327 (1987)
15. Kamal, O., Ware, G., Houston, S., Chabries, D., Christiansen, R., Brady, J., Graham, I.: Multispectral image processing for detail reconstruction and enhancement of Maya murals from La Pasadita, Guatemala. Journal of Archaeological Science **26**(11), 1391 – 1407 (1999)
16. Kleefeld, A., Burgeth, B.: Processing multispectral images via mathematical morphology. In: Hotz, I., Schultz, T. (eds.) Visualization and Processing of Higher Order Descriptors for Multi-Valued Data. pp. 129–148. Springer International Publishing, Cham (2015)
17. Köppen, M., Nowack, C., Rösel, G.: Pareto-morphology for color image processing. In: Ersbøll, B.K. (ed.) Proc. Eleventh Scandinavian Conference on Image Analysis. vol. 1, pp. 195–202. Pattern Recognition Society of Denmark, Kangerlussuaq, Greenland (1999)
18. Ngadi, M.O., Liu, L.: Chapter 4 - hyperspectral image processing techniques. In: Sun, D.W. (ed.) Hyperspectral Imaging for Food Quality Analysis and Control, pp. 99–127. Academic Press, San Diego (2010)
19. Rouy, E., Tourin, A.: A viscosity solutions approach to shape-from-shading. SIAM Journal on Numerical Analysis **29**, 867–884 (1992)
20. Serra, J.: Anamorphoses and function lattices (multivalued morphology). In: Dougherty, E.R. (ed.) Mathematical Morphology in Image Processing. pp. 483–523. Marcel Dekker, New York (1993)
21. Serra, J.: The false colour problem. In: Wilkinson, M.H.F., Roerdink, J.B.T.M. (eds.) Mathematical Morphology and Its Application to Signal and Image Processing, Proceedings of the 9th International Symposium on Mathematical Morphology, Lecture Notes in Computer Science, vol. 5720, pp. 13–23. Springer, Heidelberg (2009)
22. Tsakanikas, P., Pavlidis, D., Nychas, G.J.: High throughput multispectral image processing with applications in food science. PLOS ONE **10**(10), 1–15 (2015)
23. Unay, D.: Multispectral image processing and pattern recognition techniques for quality inspection of apple fruits. Presses univ. de Louvain (2006)
24. van den Boomgaard, R.: Mathematical Morphology: Extensions Towards Computer Vision. Ph.D. thesis, University of Amsterdam, The Netherlands (1992)
25. van den Boomgaard, R.: Numerical solution schemes for continuous-scale morphology. In: Nielsen, M., Johansen, P., Olsen, O.F., Weickert, J. (eds.) Scale-Space Theories in Computer Vision, Lecture Notes in Computer Science, vol. 1682, pp. 199–210. Springer, Berlin (1999)
26. Yang, C.C., Chao, K., Chen, Y.R.: Development of multispectral image processing algorithms for identification of wholesome, septicemic, and inflammatory process chickens. Journal of Food Engineering **69**(2), 225–234 (2005)
27. Yeh, C.: Colour morphology and its approaches. Ph.D. thesis, University of Birmingham, UK (2015)
28. Yoon, S.C., Park, B.: Hyperspectral image processing methods. In: Park, B., Lu, R. (eds.) Hyperspectral Imaging Technology in Food and Agriculture, pp. 81–101. Springer, New York (2015)